Peertechz


LIFE SCIENCES GROUP

INTERNATIONAL JOURNAL OF
Nanomaterials, Nanotechnology and Nanomedicine
OPEN ACCESS JOURNAL

ISSN: 2455-3492 DOI: https://dx.doi.org/10.17352/ijnnn

Research Article

# Dimethyl Fumarate Sterically Stabilized Solid Lipid Nanoparticles. Physicochemical properties and *in vitro* drug release

**Gisela Bevilacqua Rolfsen Ferreira da Silva[1,2]*, Guedmiller Souza de Oliveira[3], Ariana de Souza Moraes[1], Livia Rodrigues Francischini[1], Eryvaldo Socrates Tabosa do Egito[4], Fábio de Lima Leite[1] and Anselmo Gomes de Oliveira[2]**

[1]Nanoneurobiophysics Research Group, Department of Physics, Chemistry and Mathematics, Federal University of São Carlos, UFSCAR, Sorocaba, São Paulo, Brazil

[2]School of Pharmaceutical Sciences, UNESP–Sao Paulo State University, Department of Drugs and Medicines, Araraquara, São Paulo, Brazil

[3]Institute of Chemistry, Federal University of Uberlândia, Avenida João Naves de Ávila, 2121, Bloco 5T, sala 204, Uberlândia 38400-902, Minas Gerais, Brazil

[4]Federal University of Rio Grande do Norte, UFRN, Graduate Program in Health Sciences, Natal, RN, Brazil

**Received:** 06 February, 2025
**Accepted:** 01 March, 2025
**Published:** 03 March, 2025

***Corresponding author:** Gisela Bevilacqua Rolfsen Ferreira da Silva, State of Sao Paulo University (UNESP), School of Pharmaceutical Sciences, Rod. Araraquara-Jaú, km 01, Postal Code 14800-903, Araraquara, SP, Brazil,
E-mail: giselarolfsen@yahoo.com.br

**Keywords:** Sterically stabilized SLNs; Dimethyl fumarate; Hydrogenated Soy phosphatidylcholine; Poloxamer® 188; Glyceryl monostearate



https://www.chemisgroup.us

Check for updates

## Abstract

In this work Dimethyl Fumarate (DMF)-loaded and DMF-unloaded Solid Lipid Nanoparticles (SLNs) were developed and characterized by Dynamic Light Scattering (DLS), Atomic Force Microscopy (AFM), Scanning Electron Microscopy (SEM), Differential Scanning Calorimetry (DSC), and X-ray Diffraction (XRD). *In vitro* release assay was also performed, and DMF was quantified by GC-MS. SLNs were prepared by a two-step methodology using hot nanoemulsification followed by ultrasound irradiation. The results of the mean diameter, the polydispersity, and the zeta potential were in the range of 157 to 525 nm, 0.20 to 0.6, and -30 to -7mV, respectively. SLNs with spherical and elliptical shapes were evidenced by AFM and SEM techniques. XRD and DSC analyses revealed a strong interaction among the SLN components and a significant loss of crystallinity of the set of these components in the structured SLNs. Encapsulation efficiency up to 99% and loading capacity dependent on the O/S ratio has been achieved. The *in vitro* release of DMF was also dependent on the O/S ratio and could be analyzed by first-order kinetics.



**Citation:** Ferreira da Silva GBR, de Oliveira GS, de Souza Moraes A, Francischini LR, Tabosa do Egito ES, de Lima Leite F, et al. Dimethyl Fumarate Sterically Stabilized Solid Lipid Nanoparticles. Physicochemical properties and *in vitro* drug release. Int J Nanomater Nanotechnol Nanomed. 2025;11(1):015-026. Available from: https://dx.doi.org/10.17352/2455-3492.000070

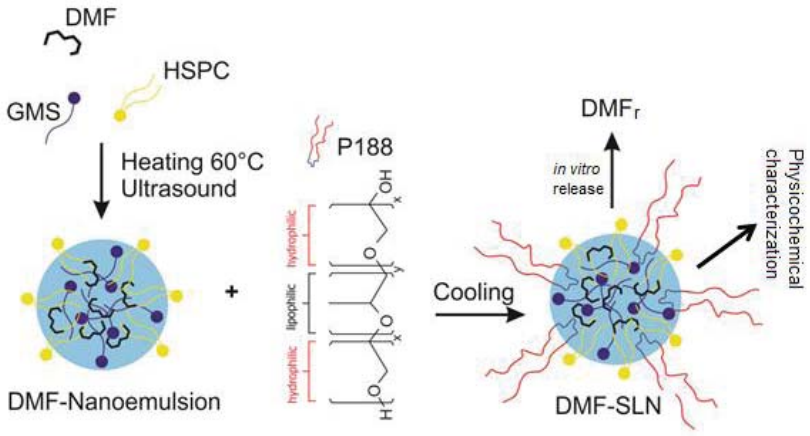


Graphical Abstract (Created using Microsoft PowerPoint).

## Introduction

Multiple Sclerosis (MS) is an autoimmune inflammatory disease of the Central Nervous System (CNS) characterized by neuroinflammation and destruction of the myelin sheath [1]. The disease is of high incidence in the adult female. The symptoms include numbness, impaired vision, balance loss, weakness, bladder dysfunction, and psychological changes [2,3]. Nowadays, there is no efficient treatment for healing MS, but the time of disease progression can be controlled through treatment [4].

Dimethyl Fumarate (DMF) has been used, by oral route, to treat the relapse rate and time to disease progression of MS [4]. However, DMF undergoes strong first-pass metabolism being partially hydrolyzed by plasma esterase to Monomethyl Fumarate making it more resilient [5]. To circumvent this problem, the Intranasal (IN) route has been proposed as an alternative to avoid the first-pass metabolism allowing the drug to easily reach the CNS providing the condition of an effective treatment for MS [6,7].

However, the DMF compound, with a molar weight of 144g/mol and a melting point of 103~104 ℃, is a crystalline sparingly water-soluble drug [8]. This molecule showed moderate-to-high permeability (apparent permeability [Papp] ≥2.3-29.7 x 10-6 cm/s, across a Caco-2 cell monolayer [9]). Despite its effectiveness, DMF has been reported as a challenging drug due to problems of multiple-dose administration and lower brain permeability, causing less patient compliance [10]. Thus, the improvement of its physicochemical properties for intranasal absorption is of utmost importance.

It is widely known in the literature that the structural disorganization of a molecule, allowed by the amorphous state, induced an increase in the apparent solubility of the drugs, allowing a better dissolution rate and, by extension, better in vivo absorption of them [11,12]. Therefore, the compartmentalization of DMF in amorphous lipid delivery systems, based on a nanotechnology platform that can allow the drug to reach the brain is of obvious relevance. Among these systems micro- and nanoemulsions [13,14], and derived systems as solid lipid nanoparticles [15-17] were widely studied. These systems have been successfully used for a wide range of drugs, including antitumor agents [18], anti-inflammatories [19], antibiotics [20], hormones [21], proteins [22], monoclonal antibodies [23], and nucleic acids [24].

Solid Lipid Nanoparticles (SLNs), mainly those sterically stabilized, can serve this purpose due to their ability to carry lipophilic drugs and modulate their release over time. SLN of structurally composed of solid lipids, and surfactants, and also has some cases, it has, also, surface-modifying substances, such as thermosensitive block copolymers. All these components are biocompatible compounds, which can be safely used in such systems [25,26].

SLNs have also been used as drug target systems for topical and systemic therapies due to their advantages over other colloidal carriers. For instance, it includes good tolerability, increased drug stability, the ability to incorporate drugs with different physicochemical properties, and the possibility of use on all routes of administration, including intravenous and intranasal routes [7,27].

Recently, our research team demonstrated that the DMF incorporated into SLNs was as effective as free DMF in reducing the clinical scores of the animals, but with reduced administration doses, when given subcutaneously [27]. In addition, preventive treatment with SLN-DMF partially allowed a reduction in the percentages of T and B cells, in the blood, when compared to preventive treatment with free DMF, orally administered, which suggests a reduction of lymphopenia [28]. The potential effects of SLNs containing DMF, administered by inhalation, on the clinical signs of the inflammatory response in the Central Nervous System (CNS) and on the changes in the lung function, in mice with Experimental Autoimmune Encephalomyelitis (EAE) were also evaluated. Indeed, the inhalation of encapsulated DMF revealed that SLN is an effective therapeutic protocol that reduces not only the CNS inflammatory process and disability progression, characteristic of EAE disease but also protects mice from lung inflammation and pulmonary dysfunction [29].



**Citation:** Ferreira da Silva GBR, de Oliveira GS, de Souza Moraes A, Francischini LR, Tabosa do Egito ES, de Lima Leite F, et al. Dimethyl Fumarate Sterically Stabilized Solid Lipid Nanoparticles. Physicochemical properties and *in vitro* drug release. Int J Nanomater Nanotechnol Nanomed. 2025;11(1):015-026. Available from: https://dx.doi.org/10.17352/2455-3492.000070

Although demonstrating the effectiveness of the DMF on SLNs, these authors [28,29] did not deeply explore the physicochemical properties of the produced DMF-SLNs. Therefore, the aim of this work was to reproduce the DMF-loaded and DMF-unloaded SLNs and physicochemically characterize them by Dynamic Light Scattering (DLS), Atomic Force Microscopy (AFM), Scanning Electron Microscopy (SEM), Differential Scanning Calorimetry (DSC), and X-ray Diffraction (XRD). The *in vitro* release profiles of DMF from the SLNs were also performed. The quantitation of the DMF on this assay was followed by GC-MS. The SLNs were produced by a two-step methodology using hot nanoemulsification/ultrasound irradiation.

## Material and methods

### Materials

Hydrogenated Soy Phosphatidylcholine (HSPC), CAS 92128-87-5, Mw 762.10 g/mol, >99% purity, was purchased from Lipoid (Ludwigshafen, Germany). Glyceryl monostearate (GMS), CAS 31566-31-1, came from Synth (Brazil). Poloxamer 188 (P188), CAS, 9003-11-6, and dimethyl fumarate (DMF), CAS, 624-49-7, were from Sigma-Aldrich (USA). Purified water, was produced from a **Millipore Milli Q Integral 3 Water Purification System,** Millipore Corporation (USA) and its resistivity was 18.2 MΩ-cm. All other chemicals and solvents were of analytical grade or better.

### Methods

**Solid Lipid Nanoparticles (SLN) preparation:** SLNs were produced (Figure 1) by hot emulsification followed by ultrasound irradiation. The surfactant blend was HSPC:P188 1:1 (w/w). P188 was dissolved in the aqueous phase and the HSPC was mixed in the lipid phase consisting of GMS and DMF. Both lipid and aqueous phases were heated, separated, at 60 °C, and subsequently homogenized to form a pre-emulsion. The pre-emulsion was, then, subjected to high-energy ultrasound for 15 minutes, (Ultrasonic Processor Model Q700, Qsonica LLC, USA) with an output frequency of 20 kHz, in a discontinuous mode (1 min. sonication and 1 min. interval) to form a hot liquid nanoemulsion, which was cooled in an ice bath to obtain SLN. Table 1 details the composition of the SLN formulations.

**Quantitative determination of DMF by GC-MS:** The DMF release was analyzed using gas chromatography and mass spectrometry (GC-MS, Shimadzu GC 2010 with AOC 5000), using an RTX-1 column (30 m x 0.32 mm; 3.0 µm film thickness), injector temperature of 250 °C, interface temperature of 270°C and injector in split mode (1:20). The column temperature started at 100 °C, and then ramped at 20 °C/min up to 250 °C. Helium gas was used as a carrier at a flow rate of 1.2 mL/min. The mass spectrometer operated with an ionization source by Electronic Interaction (EI), with an energy of 70 eV. The methodology was previously developed and validated. The determinations were carried out in triplicate.

**Encapsulation efficiency (EE) and loading capacity (LC) of the SLNs:** For EE and LC analysis, SLN formulations were diluted 100x and filtrated with Amicon® Ultra Centrifugal Filters Ultracell-50 kDa (EMD Millipore, Darmstadt, Germany) using a Heraeus™ Multifuge™ X1R centrifuge (Thermo Scientific, Waltham, MA, USA) at 3500 x g for 40 minutes at 4°C. The supernatants were collected and the DMF was quantified by CG-MS. A calibration curve of DMF in acetone (from 0,05 to 50 mg/mL) was used to determine its concentration. The determinations were performed on three independent samples.

EE and LC were calculated by the simple relationships between the quantified amount of DMF loaded in the SLN ($L_{DMF}$) by the total amount of DMF added to the SLNs ($T_{DMF}$) and the total weight of the SLN ($T_{SLN}$), respectively, using the following equations:

$$EE(\%) = \frac{L_{DMF}}{T_{DMF}} x100 \quad (1)$$

$$LC(\%) = \frac{L_{DMF}}{T_{SLN}} x100 \quad (2)$$

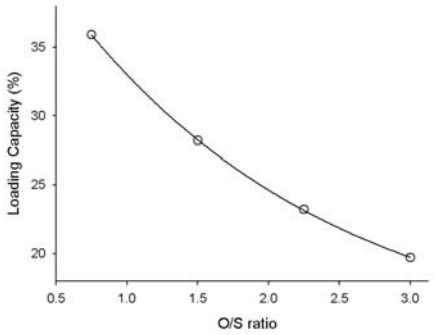


**Figure 1:** Effect of the O/S ratio on the loading capacity of SLNs.

**Table 1:** Composition of the SLNs formulations.

| SLNs | HSPC/P188 (%) | GMS (%) | DMF (%) | Aqueous phase (%) | O/S ratio |
|---|---|---|---|---|---|
| A | 2.0 | 1.5 | - | 96.5 | 0.75 |
| B | 2.0 | 3.0 | - | 95.0 | 1.50 |
| C | 2.0 | 4.5 | - | 93.5 | 2.25 |
| D | 2.0 | 6.0 | - | 92.0 | 3.00 |
| PM | 2.0 | 3.0 | - | - | - |
| $PM_{DMF}$ | 2.0 | 3.0 | 2.0 | - | - |
| $A_{DMF}$ | 2.0 | 1.5 | 2.0 | 94.5 | 0.75 |
| $B_{DMF}$ | 2.0 | 3.0 | 2.0 | 93.0 | 1.50 |
| $C_{DMF}$ | 2.0 | 4.5 | 2.0 | 91.5 | 2.25 |
| $D_{DMF}$ | 2.0 | 6.0 | 2.0 | 90.0 | 3.00 |

**Key:** (DMF) Dimethylfumarate; (SLN) Solid Lipid Nanoparticles; (P188) Poloxamer 188; (HSPC) Hydrogenated Soy Phosphatidylcoline; (GMS) Glyceryl Monostearate; HSPC/P188 (1:1); (Set A to D) DMF-unloaded SLNs; (Set $A_{DMF}$ to $D_{DMF}$) DMF-loaded SLNs. (PM) Physical mixtures; ($PM_{DMF}$) Physical mixtures loaded with DMF. Percentages expressed in w/w.

### Physical mixtures of the SLN components

Physical Mixtures (PM) were prepared in the same proportions as the SLN components with gentle homogenization of the powder mixtures (excipients) using a glass mortar. DMF was added to the PM of the inert materials and homogenized again.



**Citation:** Ferreira da Silva GBR, de Oliveira GS, de Souza Moraes A, Francischini LR, Tabosa do Egito ES, de Lima Leite F, et al. Dimethyl Fumarate Sterically Stabilized Solid Lipid Nanoparticles. Physicochemical properties and *in vitro* drug release. Int J Nanomater Nanotechnol Nanomed. 2025;11(1):015-026. Available from: https://dx.doi.org/10.17352/2455-3492.000070

**Dynamic Light Scattering (DLS):** The droplet size analysis was performed by DLS using a Zetasizer Nano system ZS (Malvern Instruments, Worcestershire, UK), with a He–Ne 4 mW laser source at 633 nm using a recording angle of 173º. The samples were diluted 1/100 (v/v) with Milli-Q purified water prior to analysis. The results represent the mean ± standard deviation of at least ten determinations. The analyses were carried out at 25 °C ± 0.2 °C. The polydispersity index was also measured. The determinations were carried out in triplicate.

**Zeta potential (ZP):** Zeta potential values were evaluated by the Laser Doppler Micro-electrophoresis Technique using a Zetasizer Nano system ZS (Malvern Instruments, Worcestershire, UK). Samples were diluted 1/100 (v/v) with purified water prior to analysis. The results represent the mean of ± SD of at least 10 determinations. The analyses were carried out at 25 °C ± 0.2 °C.

**X-ray diffraction (XRD):** XRD analysis was carried out in a Siemens (Munich, Germany) D-500 diffractometer (Cu Kα radiation, λ = 1.54056 Å) with a curved graphite monochromator, using the step-counting method (step 0.05° and time 0.1 second) in a 2θ range between 4° and 70°.

From these data, the degree of crystallinity of the samples was calculated for the physical mixtures, DMF-unloaded SLN, and DMF-loaded SLNs, according to Table 1.

The degree of sample crystallinity (Cr) was obtained through the mathematical deconvolution of the diffractogram peaks and calculated by the simple ratio between the sum of the areas of the crystalline peaks (Acryst) divided by the sum of the areas of the crystalline peaks and amorphous halos (Amorph), as shown in equation 3.

$$Cr(\%) = \left( \frac{\Sigma Acryst}{\Sigma Aamorph + Acryst} \right) * 100 \quad (3)$$

**Differential Scanning Calorimetry (DSC):** DSC analyses were carried out in a DSC 2910 Modulated DSC TA Instruments (New Castle, USA) with the range of 25 ºC - 200 ºC, under $N_2$ (100mL.min$^{-1}$), with a heating rate of 10 ºC.min$^{-1}$, using closed aluminous crucibles containing approximately 1mg of lyophilized sample. The DSC cell was calibrated before experiments using the Indium standard.

**Atomic Force Microscopy (AFM):** SLNs morphology was studied through AFM, using an Atomic Force Microscope, Bruker controller Nanoscope V. (Billerica, USA. The samples were previously dried using mica boards with the aid of nitrogen. AFM tip of nitride silicon of spring constant 0.03 N/m, in contact mode, was used. The analyses of the images were performed with the WSxM, (v. 5.0, develop 8.2) [30] and the Gwyddion software (v. 2.45) [31].

**Scanning Electron Microscopy (SEM):** The SLN morphology was also evaluated through SEM with an electron microscopy model EVOMA15 from Zeiss (Oberkochen, Germany). The SLNs were previously lyophilized and covered with gold. This metallization process was carried out on the equipment Sputter Coater BAL-TEC SCD 050 **(Leica Biosystems GmbH, Germany).**

***In vitro* release:** The *in vitro* release of DMF was performed using a Franz diffusion cells assembly in Microette Plus Hanson equipment (Hanson Research Corporation, Chatsworth, CA, USA) with a synthetic membrane of cellulose acetate. The receiver chamber, with a volume capacity of 7 mL and an effective diffusion area of 1.77 cm², was filled with an aqueous solution (saline) containing 1.5% sodium lauryl sulfate. The stirring rate and temperature were kept at 300 rpm and 37 ± 1 °C, respectively. Samples of 2 mL of drug solution were collected from the receiver chamber at the appropriate times (2, 6, 10, and 14 hours) and the volume withdrawn was replaced with a new solution medium to ensure sink conditions. The DMF released over time was determined by CG-MS as previously described. To evaluate the drug release kinetics, the experimental data were analyzed mathematically by iteration using the rules of the first-order kinetic release, a model that provided the best adjustment coefficient for the experimental data.

## Results and discussion

### Development and physicochemical properties of the SLNs

Due to the similarity of the hydrophobicity properties of DMF and SLNs, a high yield of DMF incorporation by hydrophobic effect was expected. Indeed, the high values of the EE (Table 2), in the range from 98.5 to 98.8 % (w/w), demonstrated that regardless of the values of the O/S ratio the efficiency of the DMF encapsulation remained above 98%, showing that the balance between the proportions of the oil phase and surfactant mixture was adequate for high drug encapsulation (Table 2).

On the other hand, since the LC represents the amount of drug loaded per unit of weight of the SLN and indicates the percentage of SLN mass that corresponds to the encapsulated drug, it seems rational that for situations in which the EE is close to 100%, any increase in O/S ratio should decrease the LC (Table 2).

In fact, the results showed a significant decrease in LC by an increase in the O/S ratio (Figure 1). It is important to worth that for low values of O/S ratio, the surfactant predominates over the lipid phase of SLNs, and the LC was maximum, highlighting the important role of the surfactant in the loading capacity of SLNs to encapsulate DMF (Figure 1). High EE related to lower LC values is widely reported in the literature [32].

Moreover, we evaluate the results of the mean diameter of SLNs determined by DLS. In fact, the effects of the O/S ratio as variable parameters of the SLNs in the absence and the presence of DMF were studied. The results revealed that for DMF-unloaded SLNs, the variation in the diameters was

**Table 2:** Encapsulation Efficiency and Loading Capacity.

| O/S ratio | EE (%) | LC (%) |
|---|---|---|
| 0.75 | 98.8 | 35.9 |
| 1.50 | 98.8 | 28.2 |
| 2.25 | 98.6 | 23.2 |
| 3.00 | 98.5 | 19.7 |



**Citation:** Ferreira da Silva GBR, de Oliveira GS, de Souza Moraes A, Francischini LR, Tabosa do Egito ES, de Lima Leite F, et al. Dimethyl Fumarate Sterically Stabilized Solid Lipid Nanoparticles. Physicochemical properties and *in vitro* drug release. Int J Nanomater Nanotechnol Nanomed. 2025;11(1):015-026. Available from: https://dx.doi.org/10.17352/2455-3492.000070

slightly sensitive to the O/S ratio varying between 242.2 ± 5.3 to 271.5 ± 4.5 nm. Although this variation was not significant in the process, the phenomenon can be understood because the increase in the proportion of lipids in the O/S ratio may cause natural stress in the formulation due to the increase in the local volume of the lipid core of the SLNs.

On the other hand, when decreasing the O/S ratio to minimum values in which the surfactant predominates, good conditions for the expansion of the oil-water interface of the primary nanoemulsion happens. As a consequence, an increase in the number of structured SLNs per unit volume occurs, resulting in a decrease in the average diameter. This phenomenon can be due to the ability of the stabilizing surfactant to reduce the interfacial tension of the system, allowing the formation of a more stable primary nanoemulsion that generates the SLN structures [33-35]. In addition, it was found that for DMF-loaded SLNs, the variation of the mean diameter (275.6 ± 7.5 to 298.5 ± 12.8 nm) was slightly greater than those observed for DMF-unloaded SLNs. This difference can be explained because the DMF is negligibly soluble in water and, as a consequence, it will be favorably incorporated into the lipid core, increasing the local volume of the primary nanoemulsion that generates the SLNs.

Results reporting the increase in the diameter of the structures caused by the lipophilic drug incorporation in micro and nanoemulsions and SLNs were previously reported, which is in agreement with the data of this study [7,36,37]. In general, diameters on the order of 250 nm - 400 nm, have been the most common for SLNs containing lipophilic drugs with varied compositions [38-40].

Furthermore, although the Polydispersity Index (PDI) results ranged from 0.3 - 0.5, for all experimental conditions, the size variation of SLNs is still within technologically acceptable limits. For DMF-loaded SLNs, there were no significant changes in the PDI values, also showing the good size homogeneity of the dispersed particles. Similar values of PDI were also reported for SLNs with similar compositions [7].

Concerning the zeta potential values, DMF-unloaded SLNs were in the range from -26.5 to -16.7 mV, and for 2% $_{(w/w)}$ DMF-loaded SLNs they were in the range of -29.2 ± 1.2 to -20.1 ± 0.4 mV. Nanoemulsions stabilized with phospholipid mixtures exhibiting negative zeta potential between -50 mV to -30 mV have been previously reported [41]. Negative values were attributed to the presence of phosphatidic acid and phosphatidylinositol residues, as contaminants of HSPC. In fact, zeta potentials of this magnitude (30 mV) contribute to the physical stability of particulate dispersion through electrostatic repulsion between the particles [42-44].

The experimental XRD patterns shown in Figure 2 were obtained with independent samples for the components of the SLNs, for the physical mixture at the same proportions of the SLNs, and for the DMF-unloaded and DMF-loaded SLNs. The XRD data from the single DMF showed a behavior with a very narrow-intense peak at 10.9° and the main peak at 21.92° followed by a third peak of small intensity at 27.51°, featuring the crystalline character of the drug. Pure HSPC exhibited the XRD profile with a shallow main peak and broad base at 21.24 degrees and very low-intensity signals at 6.0 and 8.84 degrees. Pure GMS presented the main peak at 23.69°, followed by two peaks of lower intensities at 19.74 and 21.65 degrees. For pure P188 the XRD pattern showed two narrow base peaks with a medium intensity at 19.06 and the main peak at 23.29 degrees, showing the crystalline nature of the substance (Figure 2a). The overall XRD data clearly reveals that all components of the SLNs, including DMF, have individual well-defined degrees of crystallinity. These profiles are similar to the data already described in the literature [45-47].

A qualitative analysis of our results reveals that regardless of the presence of DMF, an expressive degree of crystallinity remains in the physical mixture of the SLN components (Figure 2b).

Although the physical mixture still shows the clear crystallinity of the single components of the SLNs (Figures 2a,2b) when the DMF was added to it (Figure 2b) there was an increase in the intensity of the XRD diffractograms peak, narrowing at the base. This reveals the direct contribution of the drug to the increasing crystallinity of the mixture.

On the other hand, the structural organization of these components in SLNs led to a significant loss of crystallinity, revealing an intense interaction between them, mainly a low O/S ratio, in which the surfactant predominates (Figures 2c,2d). Additionally, at a high O/S ratio, a notable change in the XRD patterns from DMF was observed (Figure 2d), making it less intense and defined, suggesting a loss of the drug crystallinity.

The XRD results clearly show that in the absence of DMF the SLNs exhibit an amorphous profile at lower O/S ratios (up to 2.25), above which the proportion of lipids already predominates over the surfactant and the increased crystallinity seems to be more prominent. However, for DMF-loaded SLNs, the amorphous characteristic occurred only up to an O/S ratio of 1.5, revealing some crystallinity, thereafter (Figures 2c,2d). In fact, it is well known that the addition of surfactants to crystalline drugs produces an amorphous state or marked loss of drug crystallinity [48,49].

The results revealed that regardless of the presence of DMF, the physical mixtures of the SLN components present higher crystallinity than those of the structured SLNs. Also, the presence of DMF contributed to a small increase in crystallinity (Table 3). This aspect reveals that there was no significant interaction between these components.

On the other hand, for DMF-unloaded SLNs, the crystallinity was strongly influenced by the O/S ratio of the formulations, ranging from 12 to 32% (Figure 3), demonstrating the importance of the surfactant blend in the preparation and structuration of the primary nanoemulsion in the SLNs production processes. Additionally, it is important to note that the presence of DMF did not interfere with this profile of crystallinity, demonstrating the weak contribution of the drug to the crystallinity of the formulations.



**Citation:** Ferreira da Silva GBR, de Oliveira GS, de Souza Moraes A, Francischini LR, Tabosa do Egito ES, de Lima Leite F, et al. Dimethyl Fumarate Sterically Stabilized Solid Lipid Nanoparticles. Physicochemical properties and *in vitro* drug release. Int J Nanomater Nanotechnol Nanomed. 2025;11(1):015-026. Available from: https://dx.doi.org/10.17352/2455-3492.000070

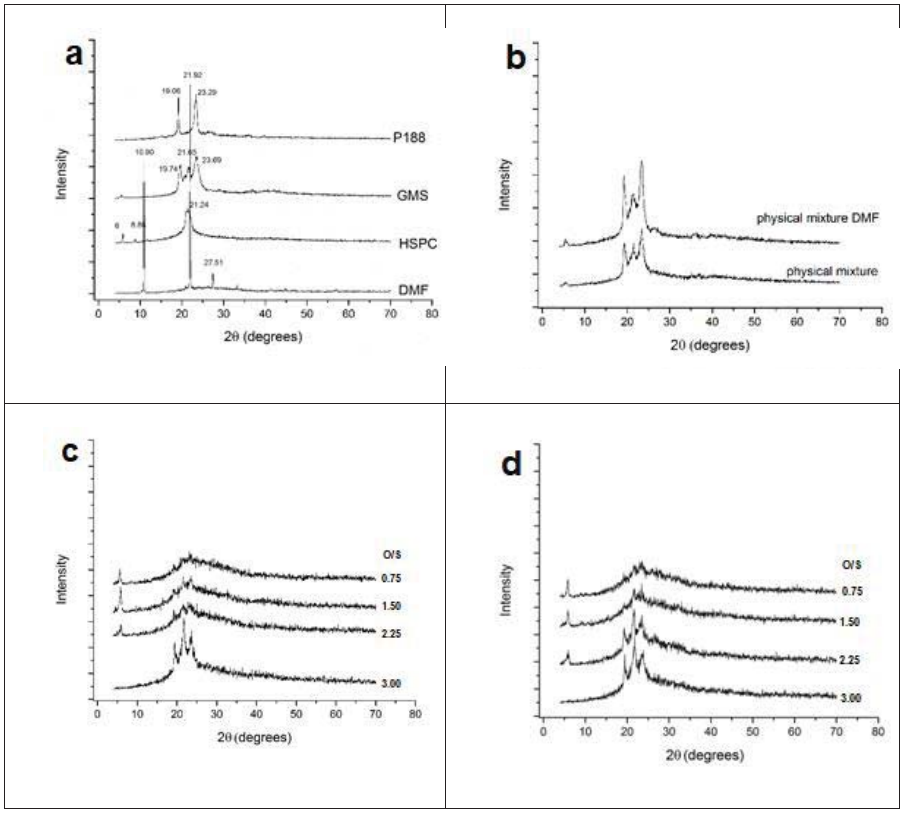


**Figure 2:** XRD diffractograms for the physical mixtures of SLN components and the structured SLNs. Key: (a) SLN Components; (b) Physical mixtures of the SLN components with and without DMF; (c) DMF-unloaded SLNs; (d) DMF-loaded SLNs. (see Table 1 for details).

However, in the presence of DMF, the crystallinity profile followed a pattern very similar to that of empty SLNs, demonstrating the weak contribution of the drug to the crystallinity of the formulations.

For both DMF-unloaded and loaded SLNs, the amorphous character was more pronounced at low values of the O/S ratio. Therefore, the proportion of surfactant, ranging from 85 to 68% with increasing O/S ratio, was quite important in producing more stable formulations, demonstrating the important role of the surfactant on the SLNs amorphization (Table 3 and Figure 3). This phenomenon is comprehensible because the increase in the O/S ratio, in addition to leading to technological stress on the primary nanoemulsion, also causes less interaction between the components of the formulations, increasing their crystallinity, as demonstrated by our experiments.

Therefore, qualitative and quantitative analyses suggest that DMF interacts with the components of the formulation, within the structured SLNs inhibiting its crystallinity, whereas in the physical mixture, there is no such interaction, and drug crystallinity remains strongly detected (Figure 3). However, in general, there was a marked predominance of the amorphous state in the SLN formulations, both in comparison with the individual components and in their physical mixtures, revealing the predominance of the amorphous state regardless of the presence of DMF.

DSC analysis results are shown in Figure 4 and summarized in Table 4. The data in Table 4 show that in the absence of

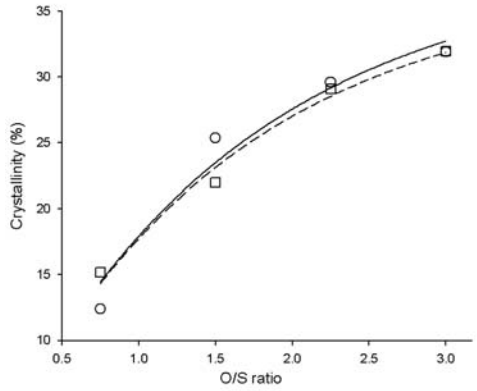


**Figure 3:** Effect of the O/S ratio on the crystallinity degree of SLNs. Key: (o) DMF-unloaded SLN; (□) DMF-loaded SLN.

**Table 3:** Crystallinity obtained from XRD analysis for Physical mixtures, DMF-unloaded, and DMF-loaded SLNs.

| SLNs | O/S ratio | Crystallinity (%) |
|---|---|---|
| A | 0.75 | 12.14 |
| B | 1.50 | 25.37 |
| C | 2.25 | 29.61 |
| D | 3.00 | 31.90 |
| PM | - | 32.89 |
| $PM_{DMF}$ | - | 37.78 |
| $A_{DMF}$ | 0.75 | 15.02 |
| $B_{DMF}$ | 1.50 | 21.95 |
| $C_{DMF}$ | 2.25 | 29.06 |
| $D_{DMF}$ | 3.00 | 31.97 |



**Citation:** Ferreira da Silva GBR, de Oliveira GS, de Souza Moraes A, Francischini LR, Tabosa do Egito ES, de Lima Leite F, et al. Dimethyl Fumarate Sterically Stabilized Solid Lipid Nanoparticles. Physicochemical properties and *in vitro* drug release. Int J Nanomater Nanotechnol Nanomed. 2025;11(1):015-026. Available from: https://dx.doi.org/10.17352/2455-3492.000070

the drug, the $T_{onset}$ was lower to the physical mixture than to the SLNs. However, concerning the $T_{peak}$ values, they were very close (60.82 and 61.0 °C), although slightly smaller than the value for the GMS (61.4 °C).

The results obtained from the GMS curve (Figure 4a) are in agreement with the literature data [50,51]. P188 shows an endothermic peak at 56.4 °C (ΔH 120.7 J/g), which is also in agreement with the literature [52].

Regardless of the variable parameters in the formulations, the enthalpy values obtained for the structured SLNs were smaller than those of the physical mixtures of the components of the formulations. Moreover, most of the DMF-unloaded SLN formulations have a $T_{peak}$ lower than the GMS $T_{peak}$ (61.5°). Therefore, it may be suggested that there was a decrease in the degree of crystallinity of the SLNs, also detected by XRD, due to the strong interaction of DMF to the lipid matrix, demonstrating that the drug was well incorporated and homogenized to it. Additionally, these results also revealed a good interaction among the components of the formulation themselves.

For both free DMF and DMF-loaded SLN, the first endothermic event comes from the melting point of the DMF, while the second event can be attributed to the drug boiling point (Figures 4a,4b). DSC curves of the DMF-loaded SLNs showed no corresponding events for both DMF melting and boiling points (Figure 4d), indicating that the drug is completely dissolved or homogeneously dispersed in the lipid matrix. The favorable interaction among the components of the formulation, as well as the complete incorporation of the drug, was also found in the results from the X-ray diffraction, which also showed the amorphous characteristic of DMF within the SLNs.

The AFM photomicrograph results show that there is a clear trend in increasing the size and changing the shape of SLNs by increasing the O/S ratio, making it elongated (Figure 5). This phenomenon can be due to the natural structural stress provoked by the increase in the proportion of the lipid phase of the primary nanoemulsion which gives rise to SLNs. Thus, an increase in the local volume of the droplets leads to an increase in the size of the final structures (Figure 5).

The AFM photomicrographs (Figure 5) and the additional data from the SEM (Figure 6) of the SLNs showed images with similar variations between spherical and elongated shapes.

The variation in the SLN composition, particularly in the O/S ratio, has a marked effect on the physicochemical properties of the studied SLNs, allowing a deep attenuation in the crystallinity. The predominance of the amorphous characteristic in the systems favored the incorporation of DMF into the lipid matrix, which certainly will play an important role in the control of *in vitro* release and *in vivo* absorption processes of the drug.

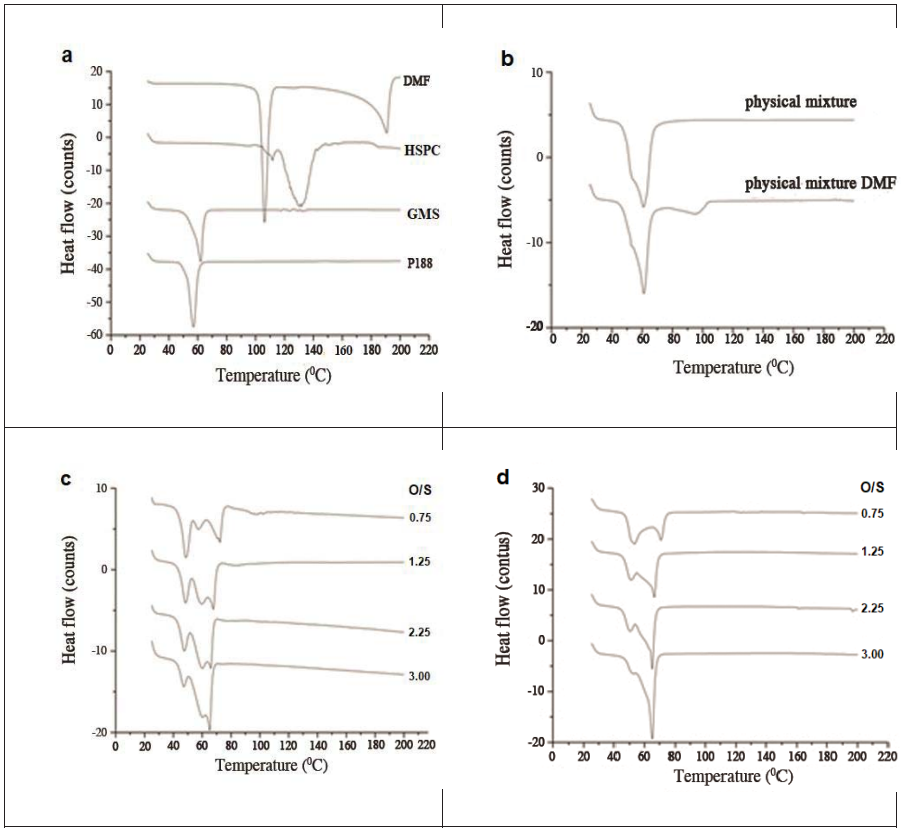


**Figure 4:** DSC curves for the physical mixtures of the SLN components and the structured SLNs. Key: (a) SLN components; (b) Physical mixtures of the SLNs components; (c) DMF-unloaded SLNs with the variation of O/S ratio; (d) DMF-loaded SLNs. (See Table 1 for details on the SLNs composition and Table 3 for formulation crystallinity details).



**Citation:** Ferreira da Silva GBR, de Oliveira GS, de Souza Moraes A, Francischini LR, Tabosa do Egito ES, de Lima Leite F, et al. Dimethyl Fumarate Sterically Stabilized Solid Lipid Nanoparticles. Physicochemical properties and *in vitro* drug release. Int J Nanomater Nanotechnol Nanomed. 2025;11(1):015-026. Available from: https://dx.doi.org/10.17352/2455-3492.000070

***In vitro* release:** The relationship between the *in vitro* release profile of DMF from SLNs and the variation in the O/S ratio is shown in Figure 7.

The release profile of all formulations reaches a plateau after approximately 10 hours (Figure 7). Also, the pattern of the release has a strong dependence on the O/S ratio. Indeed, the increase in the O/S ratio caused a marked decrease in drug release.

The DMFmax was calculated from the data in Figure 6, since in the kinetic release experiments this parameter represents the DMF that was released in infinite time.

The variation of $DMF_{max}$ against the experimental O/S ratios used is shown in Figure 8.

**Table 4:** DSC data summary of the pure substances, physical mixtures of the SLNs components, and the structured SLNs in the absence and presence of DMF.

| Sample | 1st event Melting point | | | 2nd event Boiling point | | |
|---|---|---|---|---|---|---|
| | $T_{onset}$ (°C) | $T_{peak}$ (°C) | ΔH (J/g) | $T_{onset}$ (°C) | $T_{peak}$ (°C) | ΔH (J/g) |
| DMF | 102.8 | 106.2 | 209.3 | --- | 190.8 | 257.1 |
| HSPC | 114.5 | 130.9 | 422.7 | --- | --- | --- |
| GMS | 56.0 | 61.5 | 122.9 | --- | --- | --- |
| P188 | 52.0 | 56.4 | 120.7 | --- | --- | --- |
| PM | 48.4 | 60.8 | 143.8 | --- | --- | --- |
| $PM_{DMF}$ | 53.1 | 61.0 | 168.3 | --- | --- | --- |
| A | 44.1 | 48.6 | 116.0 | 78.1 | 96.9 | 12.7 |
| B | 54.2 | 60.1 | 127.0 | 74.2 | 86.7 | 5.1 |
| C | 52.8 | 59.9 | 117.0 | 71.3 | 76.4 | 1.6 |
| D | 58.0 | 64.9 | 121.5 | 71.8 | 73.4 | 0.2 |
| $A_{DMF}$ | 53.5 | 123.3 | 119.3 | 123.4 | --- | |
| $B_{DMF}$ | 60.4 | 66.4 | 141.5 | --- | --- | --- |
| $C_{DMF}$ | 61.8 | 64.8 | 148.7 | --- | --- | --- |
| $D_{DMF}$ | 60.7 | 64.8 | 160.7 | --- | --- | --- |

**Key:** (DMF) dimethyl fumarate; (T) temperature. (PM) Physical mixtures; (GMS) Glyceryl monostearate; (HSPC) Hydrogenated Soy Phosphatidylcholine; (P188) Poloxamer P188; (Set A to D) DMF-unloaded SLNs; (Set $A_{DMF}$ to $D_{DMF}$) DMF-loaded SLNs. (PM) Physical mixtures; ($PM_{DMF}$) Physical mixtures loaded with DMF. Percentages expressed in w/w.

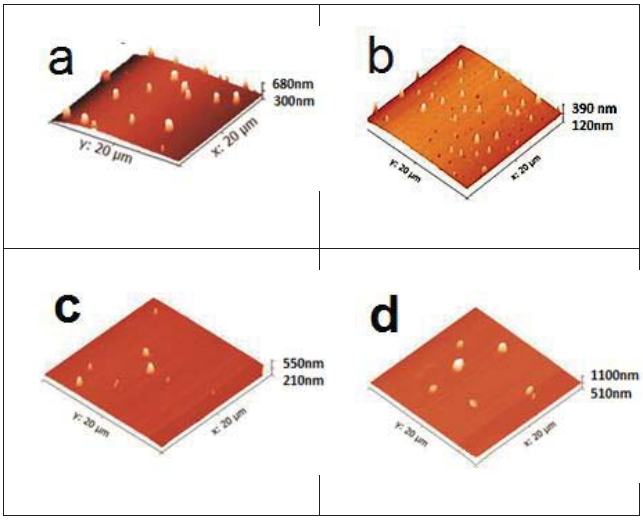


**Figure 5:** AFM photomicrographs of the DMF-loaded SLNs. Effect of the O/S ratio on the diameter at DMF 2% (w/w). Key: (a) O/S= 0.75; (b) O/S= 1.50; (c) O/S= 2.25; (d) O/S= 3.00.

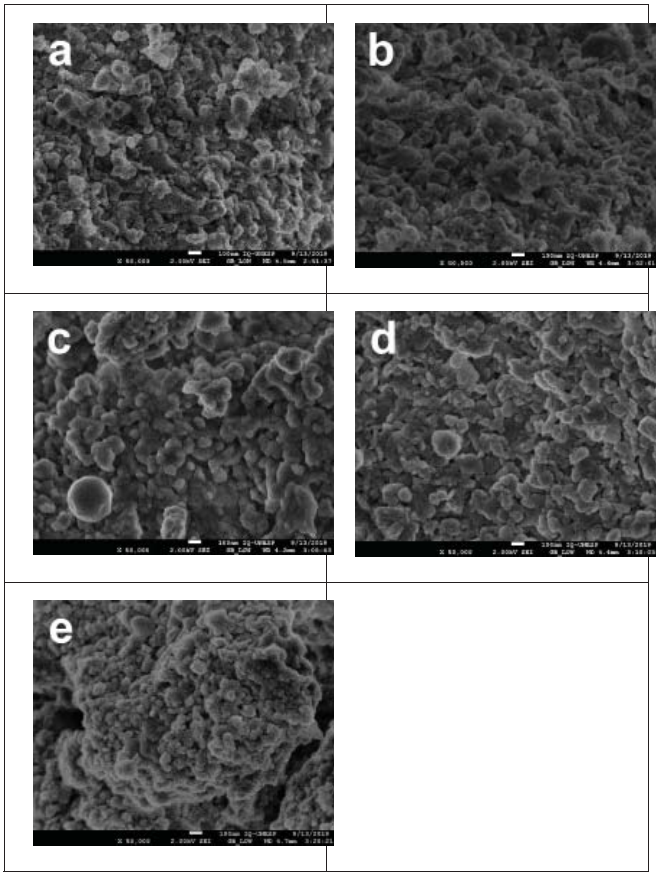


**Figure 6:** SEM photomicrographs of SLN for DMF-loaded SLNs 5% (w/w). Key: (a) O/S = 0.2; (b) O/S = 0.4; (c) O/S = 0.75; (d) O/S = 1.33; (e) O/S = 2.25.

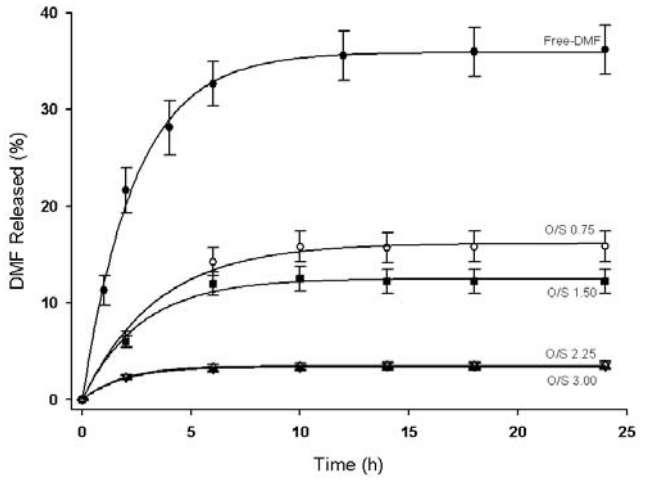


**Figure 7:** Effect of SLNs on the release of DMF from SNLs with increasing the O/S ratio in the formulations.

The decrease in the DMFmax (Figure 8) may be related to the increase in the crystallinity of the system, which is a consequence of the increase in the O/S ratio (Figure 3). This phenomenon has direct implications for the decrease in the loading capacity of the DMF in SLNs (Figure 1), inducing a strong decrease in DMFmax on drug release.

On the other hand, it is widely known that drugs and nano-structured systems such as SLNs in the amorphous state,



**Citation:** Ferreira da Silva GBR, de Oliveira GS, de Souza Moraes A, Francischini LR, Tabosa do Egito ES, de Lima Leite F, et al. Dimethyl Fumarate Sterically Stabilized Solid Lipid Nanoparticles. Physicochemical properties and *in vitro* drug release. Int J Nanomater Nanotechnol Nanomed. 2025;11(1):015-026. Available from: https://dx.doi.org/10.17352/2455-3492.000070

interact more intensely with each other, providing better incorporation, release, and absorption [53,54]. For lipophilic drugs, such as DMF, incorporated into the lipid core of SLNs, because both have similar hydrophilic-lipophilic properties, the drug will be homogeneously distributed within the lipid matrix structure, providing a homogeneous release.

In fact, the results of the DMF release from SLNs could be analyzed through a first-order model (Equation 4), which allows the extrapolation of the release data for conditions other than the experimental limits established in this work.

$$DMFr = DMFo + DMF\ (1 - e^{(-kr.t)}) \quad (4)$$

Where DMFr is the DMF released from the SLNs, DMFo is the initial DMF at time zero, kr is the release constant of DMF from SLNs, and DMF is the DMF release from SLNs in the experimental time t.

Table 5 shows the kinetic parameters obtained from the plot of the *in vitro* release curves of the DMF. The data are in agreement with the results of the loading capacity of DMF by SLNs, which was dependent on the crystallinity of the formulations and the O/S ratio (Figure 3).

Aiming better understand the release kinetics trends, both cases led to a decrease in DMFmax levels in the kinetic curves due to the restriction of DMF incorporation in SLNs induced by the increase in the crystallinity and in O/S ratio (Table 5, Figures 3 and 9). Figure 9 summarizes the relationship between the release rate constants (kr) and the variable parameters of O/S ratio, Loading Capacity (LC), and crystallinity of SLNs.

In fact, as not expected, the DMF release profiles that should be favored with the increase of the amorphous state of the formulations (at low O/S ratios), occurred in an inverse way. We believe that this phenomenon is related to the decrease in the loading capacity of the SLNs, which leads to infinite drug release times reaching faster, resulting in higher rate constants, as shown in Table 5 and Figure 9. These are, therefore, release kinetics that are directly dependent on the variation of the loading capacity.

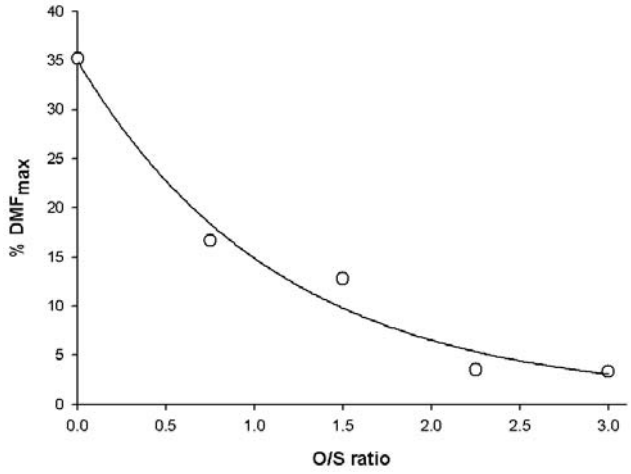


**Figure 8:** Effect of the O/S ratio on the maximum DMF released from SLNs. Data from the plot of the first-order kinetics.

**Table 5:** Fit parameters for first-order kinetic analysis of the experimental data from the DMF release of the SLN formulations.

| SLNs O/S ratio | First order kinetics | |
|---|---|---|
| | $r^2$ | $k_r (h^{-1})$ |
| 0.75 | 0.9916 | 0.2760 |
| 1.50 | 0.9920 | 0.4152 |
| 2.25 | 0.9998 | 0.5338 |
| 3.00 | 0.9968 | 0.5581 |

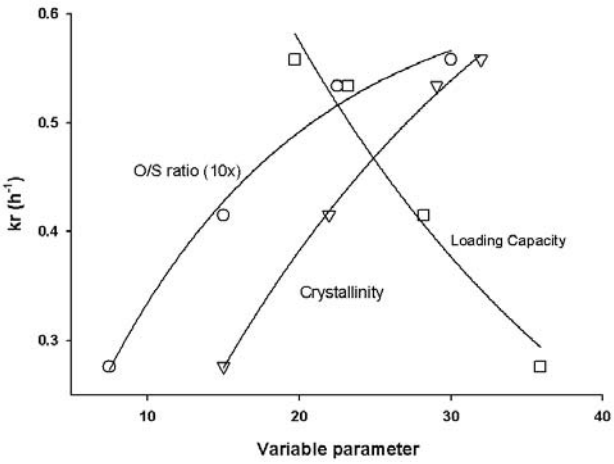


**Figure 9:** Effect of the O/S ratio, crystallinity, and loading capacity on the release rate constants of DMF from SLNs. Key: (o) O/S ratio; () Crystallinity; (□) Loading capacity.

In addition, the results of the loading capacity of DMF in SLNs clearly show an exponential decrease in the nanoencapsulated drug with the increase in the O/S ratio. This profile led to lower DMF concentrations within the SLNs and decreased release kinetics (Figure 9). The correlation between the DMF release rate constants (kr) with the O/S ratio, crystallinity, and loading capacity (Lc) is given through a first-order phenomenon, indicating a similar proportionality.

Streamlining, the processes of incorporating DMF into SLNs and the *in vitro* release from SLNs, is represented in Scheme 1.

Where (Ks) is the incorporation constant of DMF into SLNs; ($k_f$) is the DMF release constant of the drug from SLNs to be concentrated at the membrane surface; (kr) is the DMF release constant that has passed through the membrane to the equipment collect chamber.

In the overall process of drug release, according to Scheme I, the first step involves the interaction between the free DMF to the SLNs, forming the DMF-SLN that is driven by the association constant Ks, which is related to the intensity of the hydrophobic interaction between the DMF and the hydrophobic structural material of the SLNs. The second step shows that the *in vitro* release process occurs by leaving the DMF from the SLN structure, producing $DMF_f$, which depends on the rate constant $k_f$. Subsequently, the permeation of $DMF_f$ happens through the membrane, which depends on the kr permeation



**Citation:** Ferreira da Silva GBR, de Oliveira GS, de Souza Moraes A, Francischini LR, Tabosa do Egito ES, de Lima Leite F, et al. Dimethyl Fumarate Sterically Stabilized Solid Lipid Nanoparticles. Physicochemical properties and *in vitro* drug release. Int J Nanomater Nanotechnol Nanomed. 2025;11(1):015-026. Available from: https://dx.doi.org/10.17352/2455-3492.000070

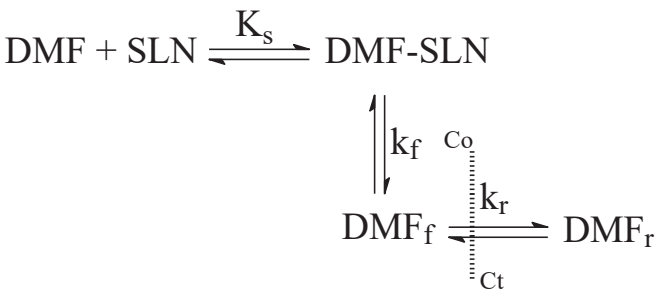


**Scheme I.**

constant, generating the $DMF_r$ in the permeation apparatus collect chamber.

Thus, the drug release depends on the interrelated constants of Scheme I, whose partial contributions will determine the overall release profile. We can rationalize that if the magnitude of kr > kf, the drug will exit from the SLNs, and no accumulation of drug at the membrane surface will occur. Therefore, the SLNs will be able to control the entire *in vitro* release process.

The kinetic results clearly demonstrate that DMF was incorporated into the SLNs by hydrophobic interaction (Scheme 1) and that the proportion of surfactant in the formulations plays a key role in *in vitro* release. This phenomenon can be demonstrated by the kinetic studies shown in Figure 7, as the experimental data of the release kinetics for all O/S ratios could be fitted through the first-order model equations and show homogeneous release throughout all kinetics.

In summary, the kinetic results clearly show that the variation of the O/S ratio on the SLN formulations has a direct impact on the loading capacity of the DMF drug, which causes important changes in the kinetic curves of the *in vitro* release due to substantial changes in the first-order rates constants.

## Conclusion

The SLN production method using nanomulsification followed by cooling under agitation was efficient and simple. Encapsulation efficiency was over 98% while loading capacity decreased with the loss of amorphous character. DMF nanoencapsulation depended on the O/S ratio, with better incorporation when surfactant predominated. SLNs showed amorphous characteristics at low O/S ratios and lost at high O/S ratios. SLNs had good diameter, zeta potential, and polydispersity index. AFM and SEM revealed spherical and elongated nanoparticles. High O/S ratios led to particle agglomeration. DMF release from SLNs was homogeneous and controllable by O/S ratio, with a first-order model fitting best ($r^2$ = 0.99).

## Acknowledgment

This work was supported by the São Paulo State Research Support Foundation – FAPESP [2013/22141-5, 2016/14264-8], XSEDE [TG-MCB150100], the National Research Council-CNPq-Brazil, and the Coordination for the Improvement of Higher Education Personnel - CAPES, for the Institutional support, grant number [001].

## References

1. Olejnik P, Roszkowska Z, Adamus S, Kasarełło K. Multiple sclerosis: a narrative overview of current pharmacotherapies and emerging treatment prospects. Pharmacol Rep. 2024;76(5):926-943. Available from: https://doi.org/10.1007/s43440-024-00642-0

2. Locatelli G, Stangel M, Rooks D, Boesch J, Pierrel E, Summermatter S. The therapeutic potential of exercise for improving mobility in multiple sclerosis. Front Physiol. 2024; 15:1477431. Available from: https://doi.org/10.3389/fphys.2024.1477431

3. Makkawi S, Maglan A, Khojah O, Allaf F, Alamoudi S, Ahmed ME, et al. Patterns of multiple sclerosis presentation to the emergency department. Front Neurol. 2024;15:1395822. Available from: https://doi.org/10.3389/fneur.2024.1395822

4. Lee DH, Stangel M, Gold R, Linker RA. The fumaric acid ester BG-12: a new option in MS therapy. Expert Rev Neurother. 2013;13:951–8. Available from: https://doi.org/10.1586/14737175.2013.814958

5. Sánchez-Sanz A, Coronado-Albi MJ, Muñoz-Viana R, García-Merino A, Sánchez-López AJ. Neuroprotective and Anti-Inflammatory Effects of Dimethyl Fumarate, Monomethyl Fumarate, and Cannabidiol in Neurons and Microglia. Int J Mol Sci. 2024;25(23):13082. Available from: https://doi.org/10.3390/ijms252313082

6. Zheng Y, Cui L, Lu H, Liu Z, Zhai Z, Wang H, et al. Nose to Brain: Exploring the Progress of Intranasal Delivery of Solid Lipid Nanoparticles and Nanostructured Lipid Carriers. Int J Nanomedicine. 2024;19:12343-12368. Available from: https://doi.org/10.2147/ijn.s497480

7. Joshi AS, Patel HS, Belgamwar VS, Agrawal A, Tekade AR. Solid lipid nanoparticles of ondansetron HCl for intranasal delivery: development, optimization and evaluation. J Mater Sci Mater Med . 2012;23:2163–75. Available from: https://doi.org/10.1007/s10856-012-4702-7

8. Weast RC, Lide DR. CRC Handbook of Chemistry and Physics. 70Th ed. CRC Press, Boca Raton; 1990.

9. Aubets J, Jansat JM, Salva M, Birks VM, Cole RJ, Lewis J, et al. No evidence for interactions of dimethylfumarate (DMF) and its main metabolite monomethylfumarate (MMF) with human cytochrome P450 (CYP) enzymes and the P-glycoprotein (P-gp) drug transporter. Pharmacol Res Perspect. 2019;7:e00540. Available from: https://doi.org/10.1002/prp2.540

10. Kumar P, Sharma G, Kumar R, Malik R, Singh B, Katare OP, et al. Enhanced Brain Delivery of Dimethyl Fumarate Employing Tocopherol-Acetate-Based Nanolipidic Carriers: Evidence from Pharmacokinetic, Biodistribution, and Cellular Uptake Studies. ACS Chem Neurosci. 2017;8:860–5. Available from: https://doi.org/10.1021/acschemneuro.6b00428

11. Alonzo D, Zhang G, Zhou D, Gao Y, Taylor L. Understanding the Behavior of Amorphous Pharmaceutical Systems during Dissolution, Pharm. Res . 2010;27:608–18. Available from: https://doi.org/10.1007/s11095-009-0021-1

12. Newman A, Knipp GY, Zografi G. Assessing the performance of amorphous solid dispersions. J Pharm Sci101. 2012;1355–77. Available from: https://doi.org/10.1002/jps.23031

13. Silva GBRF, Scarpa MV, Rossanezi G, Egito ES, Oliveira AG. Development and characterization of biocompatible isotropic and anisotropic oil-in water colloidal dispersions as a new delivery system for Methyl Dihydro Jasmonate antitumor drug. Int J Nanomedicine. 2014;9:867–76. Available from: https://doi.org/10.2147/ijn.s46055

14. Silva GBRF, M. V Scarpa, Carlos IZ, Quilles MB, Lia RC, Egito EST, et al. Oil-in-water biocompatible microemulsion as a carrier as a carrier for antitumor drug compound Methyl Dihydro Jasmonate. Int J Nanomedicine. 2015;10:585–94. Available from: https://doi.org/10.2147/ijn.s67652



**Citation:** Ferreira da Silva GBR, de Oliveira GS, de Souza Moraes A, Francischini LR, Tabosa do Egito ES, de Lima Leite F, et al. Dimethyl Fumarate Sterically Stabilized Solid Lipid Nanoparticles. Physicochemical properties and *in vitro* drug release. Int J Nanomater Nanotechnol Nanomed. 2025;11(1):015-026. Available from: https://dx.doi.org/10.17352/2455-3492.000070

15. Singh AV, Khare M, Gade WN, Zamboni P. Theranostic Implications of Nanotechnology in Multiple Sclerosis: A Future Perspective. Review, Autoimmune Dis. 2012;1–12. Available from: https://doi.org/10.1155/2012/160830

16. Bevilacqua Rolfsen Ferreira da Silva G, Pereira das Neves S, Roque Oliveira SC, Marques F, Gomes de Oliveira A, de Lima Leite F, et al. Comparative effectiveness of preventive treatment with dimethyl fumarate-loaded solid lipid nanoparticles and oral dimethyl fumarate in a mouse model of multiple sclerosis. J Autoimmun. 2022;132:102893. Available from: https://doi.org/10.1016/j.jaut.2022.102893

17. Llaguno-Munive M, Vazquez-Lopez MI, Garcia-Lopez P. Solid Lipid Nanoparticles, an Alternative for the Treatment of Triple-Negative Breast Cancer. Int J Mol Sci. 2024; 25(19):10712. Available from: https://doi.org/10.3390/ijms251910712

18. Yeo S, Jung S, Kim H, Ahn JH, Hwang SJ. 4-Hexylresorcinol Loaded Solid Lipid Nanoparticles for Enhancing Anticancer Activity. Pharmaceuticals (Basel). 2024;17(10):1296. Available from: https://doi.org/10.3390/ph17101296

19. Khishvand MA, Yeganeh EM, Zarei M, Soleimani M, Mohammadi M, Mahjub R. Development, Statistical Optimization, and Characterization of Resveratrol-Containing Solid Lipid Nanoparticles (SLNs) and Determination of the Efficacy in Reducing Neurodegenerative Symptoms Related to Alzheimer's Disease: In Vitro and In Vivo Study. Biomed Res Int. 2024; 2024:7877265. Available from: https://doi.org/10.1155/2024/7877265

20. Arabestani MR, Bigham A, Kamarehei F, Dini M, Gorjikhah F, Shariati A, et al. Solid lipid nanoparticles and their application in the treatment of bacterial infectious diseases. Biomed Pharmacother. 2024; 174:116433. Available from: https://doi.org/10.1016/j.biopha.2024.116433

21. Abou-Taleb HA, Fathalla Z, Naguib DM, Fatease AA, Abdelkader H. Chitosan/Solid-Lipid Nanoparticles Hybrid Gels for Vaginal Delivery of Estradiol for Management of Vaginal Menopausal Symptoms. Pharmaceuticals (Basel). 2023;16(9):1284. Available from: https://doi.org/10.3390/ph16091284

22. Mehrdadi S. Lipid-Based Nanoparticles as Oral Drug Delivery Systems: Overcoming Poor Gastrointestinal Absorption and Enhancing Bioavailability of Peptide and Protein Therapeutics. Adv Pharm Bull. 2024;14(1):48-66. Available from: https://doi.org/10.34172/apb.2024.016

23. Kuo YC, Ko HF. Targeting delivery of saquinavir to the brain using 83-14 monoclonal antibody-grafted solid lipid nanoparticles. Biomaterials. 2013;34:4818–30. Available from: https://doi.org/10.1016/j.biomaterials.2013.03.013

24. Fàbregas A, Prieto-Sánchez S, Suñé-Pou M, Boyero-Corral S, Ticó JR, García-Montoya E, et al. Improved formulation of cationic solid lipid nanoparticles displays cellular uptake and biological activity of nucleic acids. Int J Pharm. 2017;516:39–44. Available from: https://doi.org/10.1016/j.ijpharm.2016.11.026

25. Müller R, Maaben S, Weyhers H, Mehnert W. Phagocytic uptake and cytotoxicity of solid lipid nanoparticles (SLN) sterically stabilized with Poloxamine 908 and Poloxamer 407. J Drug Target. 1996;4:161–70. Available from: https://doi.org/10.3109/10611869609015973

26. Weyhers H, Mehnert W, Souto EB. Surface Modified Solid Lipid Nanoparticles (SLN) Analysis of Plasma Protein Adsorption Patterns by two-dimensional Polyacrylamide Gel Electrophoresis (2-D PAGE. Int J Mol Med Adv Sci. 2005;1:196–201. Available from: https://www.makhillpublications.co/files/published-files/mak-ijmmas/2005/2-196-201.pdf

27. Montenegro L, Ottimo S, Puglisi G, Castelli F, Sarpietro MG. Idebenone Loaded Solid Lipid Nanoparticles Interact with Biomembrane Models: Calorimetric evidence. Mol Pharm. 2012;9:2534–41. Available from: https://doi.org/10.1021/mp300149w

28. B. F Pinto, Ribeiro LNB, Silva GBRF, Freitas CS, Kraemer L, Oliveira FMS, et al. Vol. 136, Inhalation of dimethyl fumarate-encapsulated solid lipid nanoparticles attenuate clinical signs of experimental autoimmune encephalomyelitis and pulmonary inflammatory dysfunction in mice, Clin. Sci. 2022. Available from: https://doi.org/10.1042/CS20210792

29. Silva GBRF, Neves SP, Oliveira SCR, Marques F, Oliveira AG, Leite FL, et al. Comparative effectiveness of preventive treatment with dimethyl fumarate-loaded solid lipid nanoparticles and oral dimethyl fumarate in a mouse model of multiple sclerosis. J Autoimmun. 2022;132:102893. Available from: https://doi.org/10.1016/j.jaut.2022.102893

30. Horcas I, Fernandez R, Gomez-Rodriguez JM, Colchero J, Gómez-Herrero J, Baro AM. WSXM: a software for scanning probe microscopy and a tool for nanotechnology. Review Sci Instrum. 2007;78 013705. Available from: https://doi.org/10.1063/1.2432410

31. Gwyddion: A modular program for Scanning Probe Microscopy. Data visualization and analysis. Available from: http://gwyddion.net/documentation

32. Shah RM, Eldridge DS, Palombo EA, Harding IH. Microwave-assisted microemulsion technique for production of miconazole nitrate- and econazole nitrate-loaded solid lipid nanoparticles. Eur J Pharm Biopharm. 2017;117:141–50. https://doi.org/10.1016/j.ejpb.2017.04.007

33. Varma JNR, Kumar TS, Prasanti B, Ratna JV. Formulation and characterization of pyrazinamide polymeric nanoparticles for pulmonary tuberculosis: efficiency for alveolar Macrophage Targeting. Indian J Pharm Sci. 2015;77:258–66. Available from: https://doi.org/10.4103/0250-474x.159602

34. Siekmann B, Westesen K. Submicron-sized parenteral carrier systems based on solid lipids, Pharm. Pharmacol Lett. 1992;1:123–6.

35. Olbrich C, Muller RH. Enzymatic degradation of SLN-effect of surfactant and surfactant mixtures. Int J Pharm. 1999;180:31–9. Available from: https://doi.org/10.1016/S0378-5173(98)00404-9

36. Franzini CM, Pestana KC, Molina EF, Scarpa MV, Egito EST, Oliveira AG. Structural Properties Induced by the Composition of Biocompatible Phospholipid-Based Microemulsion and Amphotericin B Association. J Biomed Nanotechnol. 2012;8:350–9. Available from: http://doi.org/10.1166/jbn.2012.1435

37. Formariz TP, Chiavacci LA, Sarmento VHV, Franzini CM, Silva Jr AA, Scarpa MV, et al. Structural changes of biocompatible neutral microemulsions stabilized by mixed surfactant containing soya phosphatidylcholine and their relationship with doxorubicin release. Colloids Surf B. 2008;63:287–95. Available from: https://doi.org/10.1016/j.colsurfb.2007.12.021

38. Esposito E, Cortesi R, Drechsler M, Fan J, Fu BM, Calderan L, et al. Nanoformulations for dimethyl fumarate: Physicochemical characterization and in vitro/in vivo behavior. Eur J Pharm Biopharm. 2017;115:285–96. Available from: http://doi.org/10.1016/j.ejpb.2017.04.011

39. Fan T, Chen C, Guo H, Xu J, Zhang J, Zhu X, et al. Design and evaluation of solid lipid nanoparticles modified with peptide ligand for oral delivery of protein drugs. Eur J Pharm Biopharm. 2014;88:518–28. Available from: https://doi.org/10.1016/j.ejpb.2014.06.011

40. Jensen LB, Magnussson E, Gunnarsson L, Vermehren C, Nielsen HM, Petersson K. Corticosteroid solubility and lipid polarity control release from solid lipid nanoparticles. Int J Pharm. 2010;390:53–60. Available from: https://doi.org/10.1016/j.ijpharm.2009.10.022

41. Torchillin V, Amijis MM. Handbook of Material for Nanomedicine. ed.1, Jenny Stanford Publishing, Singapore. 2010.

42. Nongonierma AB, Abrlova M, Fenelon MA, Kilcawley KN. Evaluation of two food grade proliposomes to encapsulate an extract of a commercial enzyme preparation by microfluidization. J Agric Food Chem. 2009;57:3291–7. Available from: https://doi.org/10.1021/jf803367b



**Citation:** Ferreira da Silva GBR, de Oliveira GS, de Souza Moraes A, Francischini LR, Tabosa do Egito ES, de Lima Leite F, et al. Dimethyl Fumarate Sterically Stabilized Solid Lipid Nanoparticles. Physicochemical properties and *in vitro* drug release. Int J Nanomater Nanotechnol Nanomed. 2025;11(1):015-026. Available from: https://dx.doi.org/10.17352/2455-3492.000070

43. Thompson AK, Singh H. Preparation of liposomes from milk fat globulemembrane phospholipids using a microfluidizer. J Dairy Sci. 2006;89:410–9. Available from: https://doi.org/10.3168/jds.s0022-0302(06)72105-1

44. Freitas C, Muller RH. Spray-drying of solid lipid nanoparticles (SLN TM. Eur J Pharm Biopharm. 1998;46:145–51. Available from: https://doi.org/10.1016/s0939-6411(97)00172-0

45. Shah MK, Madan P, Lin S. Preparation, in vitro evaluation and statistical optimization of carvedilol-loaded solid lipid nanoparticles for lymphatic absorption via oral administration, Pharm. Dev Technol. 2013;475–85. Available from: https://doi.org/10.3109/10837450.2013.795169

46. Sharma A, Jain CP, Tanwar YS. Preparation and Characterization of Solid Dispersions of Carvedilol with Poloxamer 188. J Chil Chem Soc. 2013;58:1553–7. Available from: http://dx.doi.org/10.4067/S0717-97072013000100012

47. Kolbina M, Schulte A, Hoogevest P, Körber M, Bodmeier R. Evaluation of Hydrogenated Soybean Phosphatidylcholine Matrices Prepared by Hot Melt Extrusion for Oral Controlled Delivery of Water-Soluble Drugs. AAPS Pharm Sci Tech. 2019;20,159. Available from: https://doi.org/10.1208/s12249-019-1366-3

48. Mosquera-Giraldo LI, Trasi NS, Taylor LS. Impact of surfactants on the crystal growth of amorphous celecoxib. Int J Pharm. 2014;461:251–7. Available from: https://doi.org/10.1016/j.ijpharm.2013.11.057

49. Fountaine JS, McGinity JW, Williams RO. Challenges and Strategies in Thermal Processing of Amorphous Solid Dispersions: A Review. AAPS Pharm Sci Tech. 2016;17:43–55. Available from: https://doi.org/10.1208/s12249-015-0393-y

50. Gardouh AR, Gad S, Ghonaim HM, Ghorab MM. Design and Characterization of Glyceryl Monostearate Solid Lipid Nanoparticles Prepared by High Shear Homogenization, Br. J Pharm Res. 2013;3:326–46. Available from: https://doi.org/10.9734/BJPR/2013/2770

51. Yajima T, Itai S, Takeuchi H, Kawashima Y. Determination of optimum processing temperature for transformation of glyceryl monostearate. Chem Pharm Bull. 2002;50:1430–3. Available from: https://doi.org/10.1248/cpb.50.1430

52. Rowe RC, Sheskey PJ, Quinn ME. Handbook of Pharmaceutical Excipients. 6th ed. Pharmaceutical Press, London, UK; 2009.

53. Muller RH, Mader K, Gohla S. Solid lipid nanoparticles (SLN) for controlled drug delivery - a review of the state of the art. Eur J Pharm Biopharm. 2000;50,161-177. Available from: https://doi.org/10.1016/S0939-6411(00)00087-4

54. Patel KK, Gade S, Anjum M, Kumar S, Singh SK, Maiti P, et al. Effect of penetration enhancers and amorphization on transdermal permeation flux of raloxifene-encapsulated solid lipid nanoparticles: an ex vivo study on human skin. Appl Nanosci. 2019;9:1383–94. Available from: https://doi.org/10.1007/s13204-019-01004-6





**Citation:** Ferreira da Silva GBR, de Oliveira GS, de Souza Moraes A, Francischini LR, Tabosa do Egito ES, de Lima Leite F, et al. Dimethyl Fumarate Sterically Stabilized Solid Lipid Nanoparticles. Physicochemical properties and *in vitro* drug release. Int J Nanomater Nanotechnol Nanomed. 2025;11(1):015-026. Available from: https://dx.doi.org/10.17352/2455-3492.000070